Surface-Enhanced Raman Scattering Detected Temperature Programmed Desorption: Optical Properties, Nanostructure, and Stability of Silver Film over SiO_2 Nanosphere Surfaces

Maritoni Litorja,[†] Christy L. Haynes, Amanda J. Haes, Traci R. Jensen,[‡] and Richard P. Van Duyne*

Department of Chemistry, Northwestern University, Evanston, Illinois 60208-3113

Received: January 25, 2001; In Final Form: May 2, 2001

In this work, silver film over silica nanosphere (AgFON) surfaces are shown to be thermally stable, SERS-active substrates that are suitable for use in ultrahigh vacuum (UHV) conditions. The metal FON surface is a materials general, cost-effective, and highly SERS-active surface. The SERS activity and thermal stability were investigated by adsorbing benzene, pyridine, and C_{60} onto the AgFON surface. We chose these adsorbates for the following reasons: (1) vibrational spectroscopy and temperature-programmed desorption (TPD) behavior of benzene adsorbed onto metal surfaces has been widely investigated and is a simple system to study, respectively; (2) characteristics of pyridine adsorption on the AgFON surface can be compared to a large body of previous studies; and (3) high-temperature studies of C_{60} adsorption can be performed. TPD demonstrates that the AgFON surface has two classes of adsorption sites: (1) those that mimic the behavior of single crystal surfaces and (2) defect sites with higher adsorbate binding energies. Room temperature annealing does not irreversibly destroy the SERS enhancement capability of this surface, thereby permitting for repeated use in UHV experiments. The AgFON surface morphology and localized surface plasmon resonance frequencies, as monitored by UV-vis extinction, change as the AgFON surface temperatures increases from 300 to 548 K, and the SERS activity corresponds with these changes. Because the AgFON surface is thermally stable at room temperature and retains high SERS-activity following temperature annealing to 573 K, it is unlikely that adatoms or adatom clusters play a significant role as adsorption sites supporting the chemical enhancement mechanism. Rather, one can conclude that the electromagnetic enhancement mechanism is the most likely origin of the SER spectra from benzene, pyridine, and C_{60} adsorbed on AgFON surfaces.

Introduction

Surface-enhanced Raman spectroscopy (SERS) has great potential as a molecularly specific analytical tool in ultrahigh vacuum (UHV) surface science.[1−3] One of the greatest strengths of SERS is its applicability to studies at solid/UHV, solid/liquid, and solid/solid interfaces. In addition, high spectral resolution (1 cm^{-1}), time resolution (potentially 0.1−1 ps), and the ability to reveal the bonding, orientation and identity of surface species are all strong positive attributes of SERS. However, SERS has not been fully utilized in UHV surface science applications due to the following limitations: (1) the requirement for nanoscale surface roughness features to activate SERS as compared to the single crystal substrates typically used in UHV experiments and (2) the limited thermal stability and poor structural characterization of SERS-active substrates.

SERS continues to be a widely applied technique to obtain vibrational information from surface confined molecules. Thousands of papers have been published on this subject since its discovery 24 years ago. Many excellent, comprehensive reviews on the subject are available.[2−5] Furthermore, several application-specific reviews of SERS have been written for electrochemistry,[6] medicine,[7] biochemistry,[8] and UHV surface science.[9] Although SERS has been successfully used to study many different chemical systems and is well-recognized as being one of the most sensitive molecular spectroscopies with attomole[10] and even sub-1000 molecule[11,12] detection limits, as well as molecular identification capabilities, the details of the mechanism(s) responsible for its signature observable, a 6 order magnitude increase in intensity as compared to conventional Raman scattering, are still not completely understood. As is well-known, there are two contributions to the SERS enhancement mechanism: the electromagnetic (EM) enhancement[13] and the chemical (CHEM) enhancement.[14] The EM enhancement mechanism can explain enhancement factors in the range $\sim 10^4-10^7$ and is recognized as a "long-range" effect.[2] In contrast, the CHEM enhancement mechanism is thought to be responsible for an enhancement factor $\sim 10^1-10^2$ and is viewed as an extremely short-range phenomenon requiring orbital overlap between the outermost layer of surface atoms and the adsorbate.[2,3] Recent observation of single molecule SERS signals, with total enhancement factors of 10^{14}, has both renewed the interest in the investigation of SERS enhancement mechanisms and complicated our understanding of the partitioning of the total enhancement into EM and CHEM contributions. Current experimental evidence suggests that the EM enhancement mechanism plays a large role in single molecule SERS but falls some 4−6 orders of magnitude short of accounting for an enhancement factor of 10^{14}.[15−17]

UHV−SERS experiments were initiated in 1979−1980 so that the environmental variables contributing to the SERS

* To whom correspondence should be addressed. E-mail: vanduyne@chem.nwu.edu.

[†] National Institute of Standards and Technology, Gaithersburg, MD.

[‡] Omega Optical, Inc. Brattleboro, VT.

10.1021/jp010333y CCC: $20.00
Published on Web 06/16/2001

mechanism could be isolated and systematically investigated in a highly controlled manner. A variety of surface preparation techniques were used to create randomly roughened metal surfaces in UHV with the requisite nanoscale feature sizes. Polycrystalline silver sheets bombarded by an argon ion sputtering beam produced a surface with an enhancement factor of 10^3-10^5.[18,19] Rowe and co-workers used iodine vapor and ultraviolet light to cause photochemical oxidation−reduction of the silver metal. The resulting surface roughness features, on the order of 50 nm, exhibited enhancement up to 10^4.[20,21] Although these randomly roughened surfaces exhibited sufficient enhancement factors to generate measurable SERS signals, many of the details of the EM enhancement mechanism, particularly its dependence on the excitation wavelength (λ_{ex}) and particle size, were still largely obscured due to the broad distribution of surface feature sizes.

Several research groups made use of UHV experiments in order to isolate the role of surface plasmon polaritons (SPP), a long-range EM enhancement, from the short-range CHEM enhancement mechanism. To do this, regularly structured "rough" surfaces had to be designed. For example, Sanda et al. used a holographic silver grating in a UHV−SERS experiment to measure enhancement factors as a function of adsorbate surface coverage. At maximum surface coverage, an enhancement factor of 10^4 was measured. On the basis of the decrease in Raman signal between the first and the second monolayers (ML), they deduced an enhancement factor of 10^2 attributable to the CHEM enhancement mechanism. The remaining 10^2 enhancement results from excitation of the SPP.[22] A similar experiment by Tsang et al. attributed an enhancement factor of 10^2-10^3 to SPP field enhancement.[23] These experiments were important in the ongoing enhancement mechanism debate, but the complicated sample preparation deterred other research groups from pursuing this approach.

As a straightforward alternative to silver gratings, silver island films were introduced as SERS-active substrates. Island films produced by vapor deposition of a mass thickness (d_m) between 10 and 100 nm of metal on a flat substrate, usually glass or quartz, were found to exhibit an enhancement factor of $\sim 10^4$.[24−27] These films are one of the simplest and most reproducible SERS-active surfaces to prepare. Scanning electron microscope (SEM)[28] and atomic force microscope (AFM)[29,30] images of island films (not in UHV) have shown the presence of disordered spheroidal particles 5−20 nm in diameter. Island size distributions and consequently, SERS enhancement factors were found to be highly dependent on the choice of substrate,[24] cleaning procedures,[31] and deposition parameters.[18,21,32]

When silver films were deposited in UHV at cryogenic surface temperatures of 10−100 K, they were found to exhibit SERS enhancement factors of $\sim 10^4-10^5$.[21,25,33,34] These cold-evaporated metal films (CEMFs), however, irreversibly lost all enhancement upon warming the surface to room temperature.[33,35,36] Subsequently, UHV scanning tunneling microscopy (STM) was used to demonstrate that CEMFs are composed of adsorbed fractal clusters.[9] To study structural changes in these films, the samples were annealed to 560 K and imaged with STM. These STM images show that thermally annealed surfaces lost both their fractal characteristics and their SERS activity.[37] This irreversible loss of SERS activity is highly detrimental to the application of SERS in surface science and catalysis.

From the perspective of the EM enhancement mechanism, changes in the roughness features during room-temperature annealing would shift the localized surface plasmon resonance (LSPR) frequency, thus diminishing or eliminating any EM enhancement at the excitation wavelength used. Attenuated total reflection experiments by Hemminger showed that CEMFs are metastable with respect to thermal excursion.[38] CEMFs have broad optical absorption bands at low temperatures because of the large variation in feature shape and size. As the surface is annealed, the absorption peaks become sharp and narrow due to the increased homogeneity of the surface features.

From this brief review of the literature on UHV-compatible, SERS-active surfaces, one concludes that all of these surfaces lack thermal stability. The observation of irreversible loss from CEMF surfaces, in particular, supported the adatom explanation for the CHEM enhancement mechanism. Recently, Weaver and co-workers have carried out brilliant experiments involving electrochemical SERS and gas-phase SERS of transition metal overlayer on Au.[1,39−46] To date, their potential for UHV−SERS studies has not been exploited.

An immediate and practical goal of the work presented here is to create a SERS-active surface suitable for use in UHV that is reproducible, stable, and predictable. Here, we present the use of silver film over silica nanospheres (AgFON) as the SERS-active surface that meets the above criteria and allows one to probe surface chemistry and adsorption energetics by combining temperature-programmed desorption (TPD) with SERS. In the experiments presented here, investigations of the adsorption characteristics of the AgFON surface with TPD using benzene, pyridine and C_{60} as the adsorbates were performed. Pyridine was investigated as an adsorbate so that these new results could be directly compared with the extensive body of pyridine SERS data recorded from other surfaces. However, the TPD characteristics of pyridine desorption from AgFONs were more complex than anticipated. Benzene was studied and was found to exhibit simpler desorption behavior. Consequently, significant new insights into the nature of the adsorption sites on AgFONs were obtained. C_{60} was investigated because it desorbs at a higher temperature, therefore, allowing investigation of SERS activity above ambient conditions. Observations regarding temperature effects on the surface nanostructure and its optical properties are presented using AFM and reflection mode UV−vis extinction spectroscopy.

Experimental Section

Instrumentation. A Physical Electronics model 548 UHV chamber with a base pressure of 2×10^{-10} Torr was used in these experiments. The AgFON, Ag(110), and Ag(111) surfaces were mounted on an XYZΘ, liquid nitrogen-cooled, electron beam heated manipulator. The chamber has been modified to contain one evaporation source for metal (silver) and another for volatile solids (C_{60}).

TPD spectra were collected using an IBM-compatible computer with a data acquisition board (Digital Boards) interfacing the signal from a UTI100 quadrupole mass spectrometer with the amplified and conditioned chromel−alumel (Type K) thermocouple signal. Molecular ion signals for pyridine ($m/e = 79$) and benzene ($m/e = 78$) were used in acquiring the TPD spectra. Heating rates (β) were typically 4 Ks^{-1}, and the collection frequency was 10 Hz.

AFM images of the AgFON surfaces in air were recorded using a Nanoscope II microscope (Digital Instruments) with a 12 μm scan head. Si_3N_4 cantilevers operating in constant force mode with 20 nN force and scan rate of 8 lines/s were used.

Raman spectra were obtained using the 514.5 nm line of a Spectra Physics model 2060 argon ion laser or the 632.8 nm line from a Spectra Physics model 124B HeNe laser. The input laser beam was incident at 15° and scattered radiation was

collected by a telescopic camera lens normal to the surface. The collimated output passes though a holographic edge filter (Physical optics Co. and Kaiser Optical Systems) to filter the Rayleigh line and is then focused onto the slit of an Acton VM-505 spectrograph equipped with a liquid nitrogen-cooled Photometrics PM-512 CCD detector.

UV−vis extinction spectra of the AgFON surfaces were collected using a Beckman DU-7 spectrophotometer. The samples were annealed at the desired temperature in 30 min increments prior to spectra collection.

Surface Preparation. For the samples used in these experiments, silica nanospheres (10% solids in water, Bangs Laboratories) were diluted 5:1 in a surfactant solution of Triton X-100 in methanol (1:50) and incubated at room temperature for a week prior to use. The surfactant was added to effectively disperse the nanospheres on the surface.

Nanosphere suspensions were spin-coated (ex situ) onto a polycrystalline copper substrate (1 cm × 1 cm × 2 mm) that had been polished with emery papers and alumina slurries (Buehler Polishing Co.) until mirrorlike and scratch-free. Under vacuum, the sample was annealed to 573 K several times to eliminate contaminant gases and any organic residue from the silica nanosphere production.

Silver metal (pellets, 99.99%, Johnson & Matthey) was evaporated in situ onto the nanosphere-covered sample from a home-built evaporation oven. The oven consists of a quartz tube-encased tungsten filament inside a water-cooled jacket with a shuttered conical aperture. The silver beam passes through this aperture and deposits onto the nanospherecoated sample. To ensure the deposition of the desired amount of silver for the silica nanosphere size used, the beam flux was monitored. The beam flux is intercepted and measured by a quartz crystal microbalance (QCM) (XTC Inficon). The deposition was done with a constant filament current in 3−5 min durations. Unless noted, for all experiments reported here, 160 nm (d_m = 160 nm) of silver was deposited over the 400 nm-diameter silica nanospheres (D = 400 nm).

The Ag(110) and Ag(111) surfaces were purchased from Monocrystals Co. and were polished prior to chamber mounting. Both the AgFON and the single-crystal surfaces were cleaned using Ar-ion sputtering and subsequent surface annealing to 573 K. Surface cleanliness before and after experiments was verified using Auger electron spectroscopy (AES).

Materials. Pyridine and benzene (Aldrich Chemicals) were purified using several freeze−pump−thaw cycles. C_{60} (99.9%, Kappes laboratory, Universitat Karlsruhe, Germany) was recrystallized from carbon disulfide or toluene. The silver and C_{60} ovens were degassed by repeated heating cycles. Each cycle lasted 3−5 days and was done both 1 week before use and again for 2−3 h prior to deposition. By degassing these materials before their introduction to the system, the chamber pressure never rose above the 10^{-8} Torr range during depositions.

UHV Experimental Procedure. After silver deposition, the SERS sample was cooled to 100 K and dosed by backfilling the chamber with the appropriate gas (benzene, pyridine) using a variable leak valve (Varian). Doses are expressed in uncorrected Langmuirs (L) (1 L = 1 × 10^{-6} Torr*sec). C_{60} was introduced to the chamber using sublimation techniques. Doses were monitored using the QCM. The variation of the vibrational spectrum with respect to adsorbate concentration was monitored for each adsorbate by taking sequential Raman spectra. TPD spectra collected from both new and the corresponding Raman experiment samples provided adsorbate desorption profiles from the AgFON samples. Next, TPD and SERS spectra were collected from a single sample in order to correlate adsorbate concentration with the SERS signals observed. The sample was cooled to 110 K after each annealing step before spectra were collected. For experiments with C_{60}, the surface was held at room temperature.

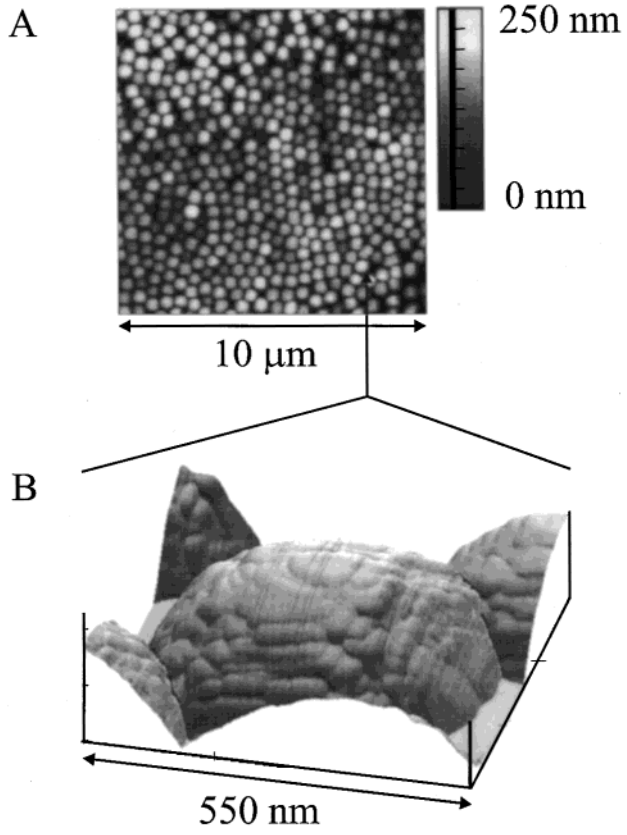

Figure 1. Contact mode AFM image of the AgFON surface (d_m = 160 nm Ag, D = 400 nm SiO_2 nanospheres). (A) Array of nanospheres over a 10 μm × 10 μm area. (B) Image showing small scale roughness on a single nanosphere. Images were taken in air.

Results and Discussion

Nanostructure of AgFON Surfaces. Silica nanospheres, in comparison to polystyrene nanospheres,[46] do not pack in as highly ordered a manner. This difference can be attributed to the broader size distribution of the silica nanospheres (10%) compared to the polystyrene nanospheres (<5%). The topography of the AgFON surface, examined by AFM (Figure 1), shows 20−50 nm substructures superimposed on the grating-like structure of the metal-covered nanosphere array. The substructure topography is dependent only on the metal evaporation rate. The highly reproducible nature of this topography, with controlled evaporation rate, is an important factor in creating SER spectra with highly reproducible intensities.

UHV−SERS from Pyridine, Benzene, and C_{60} on AgFON Surfaces. Figures 2 and 3 show the SER signals from the pyridine, benzene, and C_{60} adsorbates. The top trace in Figure 2A is that of 5 L of benzene on the AgFON surface, whereas the bottom trace is of 3000 L of benzene on the Ag(110) surface. Both the normal Raman spectrum of the thick benzene film and the SER spectrum show the presence of the $\nu_{11}(A_{2u})$ mode at 607 cm^{-1}, which is normally forbidden under the D_{6h} symmetry of the free molecule. In the top spectrum of Figure 2A, adsorption of benzene lowers its symmetry from D_{6h} to at least C_{6v}.[47] There are two peaks associated with the $\nu_1(A_{1g})$ symmetric ring-breathing mode of benzene: the more intense one at 989

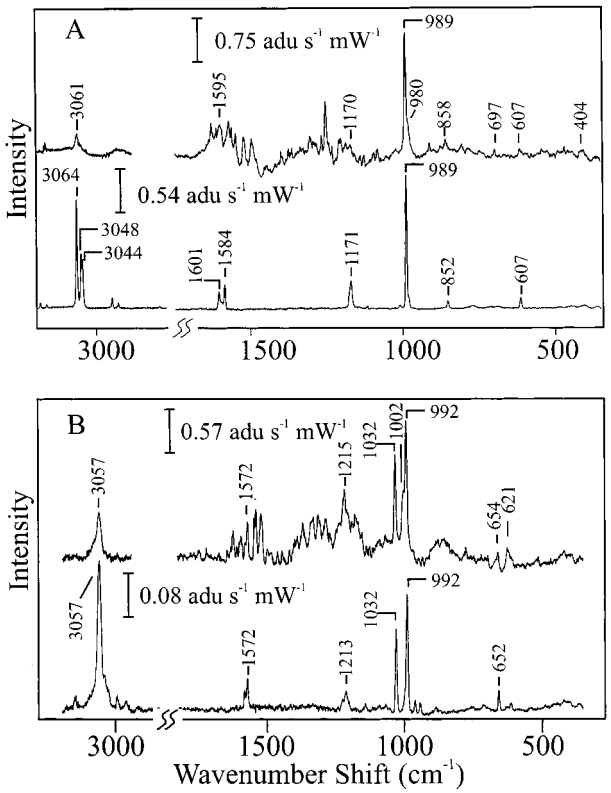

Figure 2. SER vs normal Raman spectra of benzene and pyridine. (A) SERS of 5 L of benzene on a AgFON surface (top) vs normal Raman spectrum of 3000 L of benzene on the Ag(110) surface (bottom). (B) SERS of 5 L of pyridine (top) vs normal Raman spectrum of 3000 L of pyridine on Ag(110) (bottom). Spectra were collected with 18 mW of $\lambda_{ex} = 514.5$ nm for 200 s for the SERS and 90 mW for 200 s for the thick film on Ag(110).

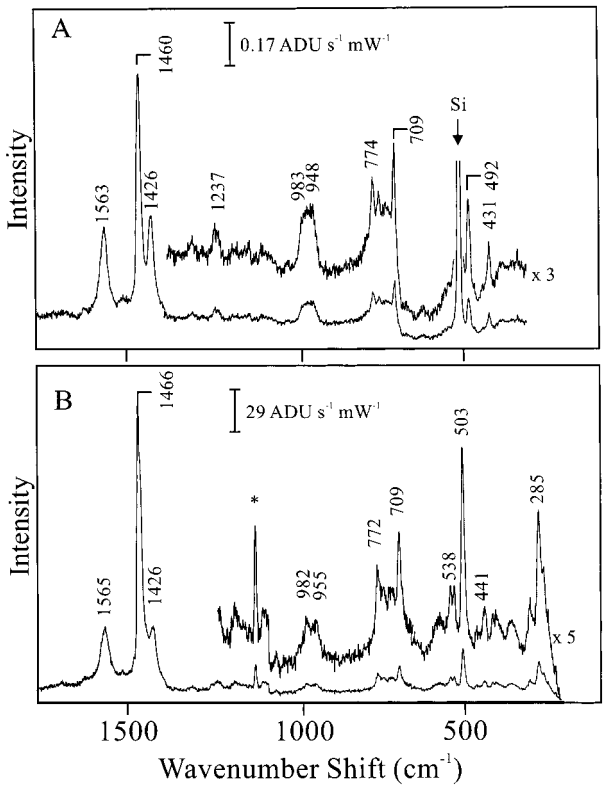

Figure 3. RRS vs SERRS of C_{60}. (A) RRS of a thick film of C_{60} on Si(100) in UHV taken with 50 mW of $\lambda_{ex} = 514.5$ nm for 300 s. (B) SERRS spectra of 1.0 ML C_{60} on AgFON taken with 7 mW of $\lambda_{ex} = 514.5$ nm for 30 s.

cm^{-1}, close to the liquid-phase value of 992 cm^{-1}, and one with a lower frequency, at 980 cm^{-1} which saturates at low coverage and appears as a shoulder on the 992 cm^{-1} peak. The appearance of the ν_1 mode at two different frequencies was also observed by Tsang et al.[23] for benzene on a silver grating and by Moskovits[48] at temperatures higher than 60 K. These two peaks have been assigned to benzene molecules adsorbed at two different surface sites: (1) flat terraces, on which the molecules are adsorbed with the molecular plane parallel to the surface, and (2) steps and defect sites, where benzene is forced to adsorb with the molecular plane perpendicular to the surface. Although the preferred conformation for many adsorbates has the molecular plane perpendicular to the surface, all published vibrational studies of adsorbed benzene conclude that it preferentially adsorbs with its molecular plane parallel to the surface.[49] A more detailed discussion of the adsorption of benzene on AgFONs is the subject of a separate publication.[50,51]

The top trace in Figure 2B is from 5 L of pyridine on the AgFON surface, whereas the bottom trace is from 3000 L of pyridine on the Ag(110) surface. The $\nu_1(A_{1g})$ symmetric ring breathing mode for pyridine also occurs at two frequencies: 1002 and 992 cm^{-1}. Campion et al. attributed the 1002 cm^{-1} peak to pyridine adsorption on defect or low coordination sites in an unenhanced surface Raman spectroscopic (USRS) study of pyridine on Ag(540).[52] The 992 cm^{-1} peak is attributed to pyridine physisorbed on the surface based on the similarity of the wavenumber shift to the liquid phase value. For pyridine adsorbed on low index faces of silver, such as that on the lower trace of Figure 2B, only the 992 cm^{-1} peak is observed. On cold-evaporated silver films,, the 1002 cm^{-1} peak dominates the spectrum and is attributed to chemisorbed pyridine on SERS-active sites.[3,33,53] Both peaks are observed on many other SERS-active surfaces such as gratings and island films. The 1002 cm^{-1} peak is observed first at low coverage, whereas the 992 cm^{-1} peak grows in at higher coverage in accord with the expectation that molecules adsorb on the higher energy sites first. From the SER spectra of pyridine and benzene, we can conclude that surface defect sites and crystalline areas coexist on AgFON surfaces.

The surface-enhanced resonance Raman spectrum (SERRS) of C_{60} is greatly enhanced (Figure 3B) compared to the corresponding resonance Raman spectrum (RRS) of a thick film of C_{60} on Si(100), shown in Figure 3A. The large peak at 1466 cm^{-1} is attributed to the pentagonal pinch mode of C_{60}. In previous work, by Moskovits and co-workers, SERR spectra were recorded in UHV from a cold-evaporated silver film.[54] On this substrate, the pentagonal pinch mode was downshifted from the solution frequency of 1460 cm^{-1} to 1436 cm^{-1}. One hypothesis for this large downshift, in disagreement with the data presented herein, is that adsorption of C_{60} onto cold-evaporated silver films induces a charge-transfer reaction, producing C_{60}^-. SER spectra of C_{60}^- on a redox roughened gold electrode, measured by Weaver et al., show the C_{60}^- pentagonal pinch mode at 1443 cm^{-1},[55] in close agreement with the Moskovits result. Another hypothesis, which cannot be ruled out, is that the C_{60} adsorption characteristics on the highly reactive CEMF causes the large frequency shift for the pentagonal pinch mode. Both hypotheses support the idea that CEMFs have a large areal density of highly reactive adatom or adatom cluster adsorption sites. The atypical behavior of C_{60} adsorption to the CEMF clearly shows the disadvantage of working with such highly reactive SERS substrates. Because the AgFON retains SERS-activity even after heating to a temperature where adatoms are eradicated, adsorbate behavior

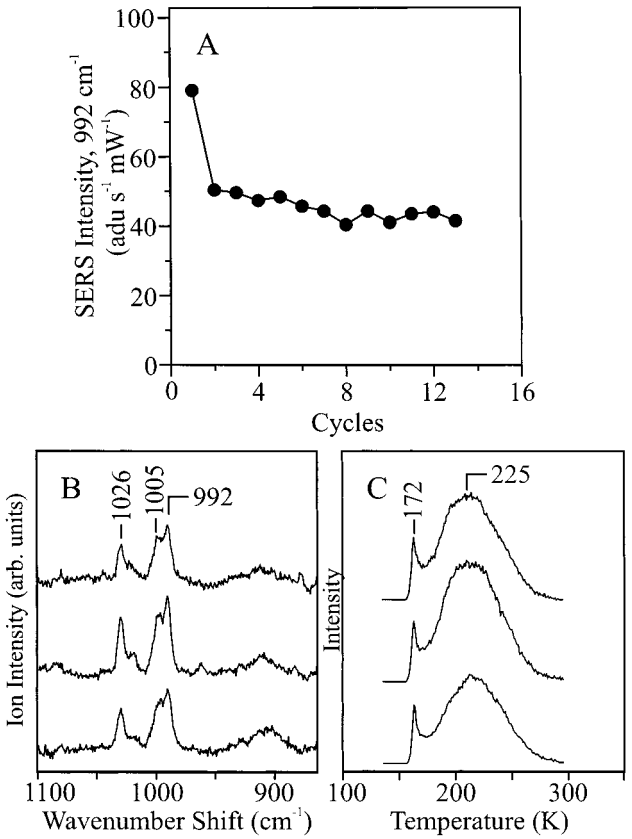

Figure 4. Stability of AgFON toward replicate adsorption−desorption cycles of benzene and pyridine. (A) SERS intensity of the 992 cm^{-1} peak of 10 L of benzene. Each cycle consists of adsorption of benzene at $T_{surf} = 110$ K and thermal desorption at 300 K with $\beta = 4$ Ks^{-1}. SERS spectra were taken with 18 mW of $\lambda_{ex} = 514.5$ nm for 60 s. (B) Replicate SERS spectra in the 900−1100 cm^{-1} region of 5 L of pyridine on the AgFON surface collected using 8 mW of $\lambda_{ex} = 632.8$ nm for 60 s. (C) The corresponding TPD spectra of pyridine desorbing from the AgFON at $\beta = 4$ Ks^{-1}.

is simpler to interpret and strong SERS enhancement is still obtained.

Thermal Stability and TPD of AgFON Surfaces. The temporal and thermal stability of the AgFON sample is illustrated in Figures 4 and 5. In Figure 4A, the variation of SERS intensity of the 992 cm^{-1} peak of benzene was monitored with successive 5 L doses. The signal dropped by 25% after the first cycle and then became approximately constant for the remaining 12 cycles. Such an equilibration procedure is typical in many surface science experiments, and in these experiments, this decrease can be regarded as a normal part of the surface preparation protocol.

Figure 4, parts B and C, shows replicate SER spectra of 5 L pyridine on the AgFON surface in the 900−1100 cm^{-1} region and the corresponding TPD spectra following each deposition, respectively. These are typical SERS and TPD spectra taken on a single sample. The occurrence of both the 992 cm^{-1} and the 1005 cm^{-1} peaks in the SER spectra support the conclusion that pyridine adsorbs at both crystalline-like (992 cm^{-1}) and defect (1005 cm^{-1}) sites. The corresponding TPD spectra show two peaks: one at 172 K, which is assigned to pyridine multilayers, and a broad peak extending from 190 K to almost 300 K which is attributed to chemisorbed pyridine. Together, the TPD and SER spectra demonstrate that this surface has both atomically crystalline and defect sites.

A combined AFM and SERS study of gold films slowly deposited on mica at 513 K revealed large atomically flat (111) domains.[56] This Au(111)/mica surface was shown to exhibit strong surface enhancement even though it was not previously believed possible. TPD spectra for 5 L of pyridine on the Ag-(111) and Ag(110) surfaces are shown in Figure 5, parts A and B, respectively. These TPD signals from the low index faces of silver single crystals aid the interpretation of the TPD spectrum of 8 L of pyridine from the AgFON surface (Figure 5C). Two desorption states are clearly revealed on the AgFON surface. The desorption temperature corresponding to more weakly bound pyridine on the AgFON surface is roughly the same as that for the main pyridine desorption signals from the Ag(111) and Ag(110). The broad, high-temperature tail of the TPD signal in Figure 5A corresponds in temperature range to the broad peak at 225 K in Figure 5C. It is hypothesized that this tail can be attributed to pyridine adsorbed to surface defect sites. The exact assignments of these peaks will be discussed in more detail in another paper.[51]

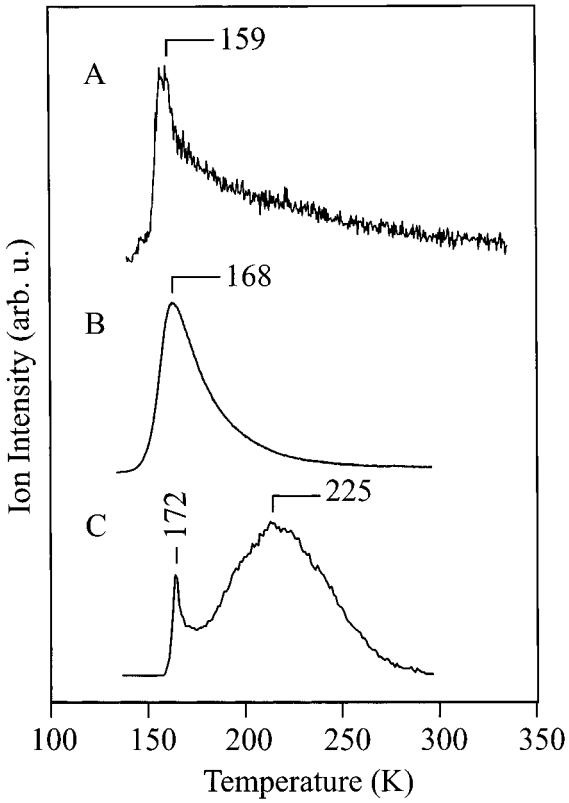

Figure 5. TPD spectra of pyridine on three Ag surfaces. (A) TPD of 5 L of pyridine on the Ag(111) surface. (B) TPD of 5 L of pyridine on the Ag(110) surface. (C) TPD of 8 L of pyridine on the AgFON surface. Spectra were collected with $\beta = 4$ Ks^{-1}.

Figure 6A shows a spectrum of 0.1 ML C_{60} on the AgFON surface taken immediately after deposition, whereas Figure 6B is the spectrum of the same sample in the UHV chamber taken 28 days later. There are no significant changes in the spectrum other than an apparent improvement in the signal-to-noise ratio. The increased signal intensity can be attributed to improved instrument alignment before the final measurement. This sample, therefore, shows remarkable temporal stability.

The AgFON can be reused many times in UHV−SERS studies. Figure 7A is the AES of the surface immediately after silver deposition, whereas Figure 7B is the spectrum after hundreds of depositions of benzene and pyridine. Although the carbon and silver peaks in the AES overlap, the surface is deemed free from carbon contamination if the ratio of the 266 eV peak to the 304 eV peak is between 0.4 and 0.5.[57] The ratio

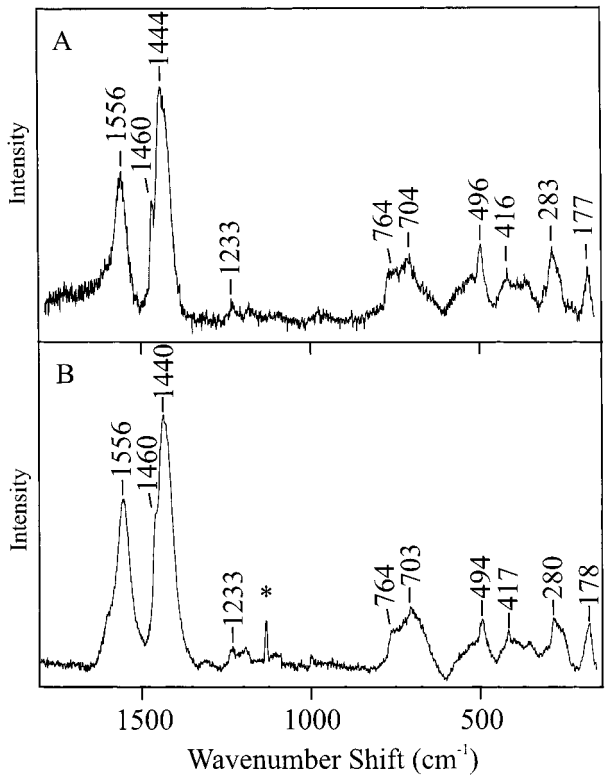

Figure 6. Temporal stability of AgFON surface. SERRS signal of 0.1 ML of C_{60} on the AgFON surface taken (A) immediately after deposition and (B) after day 28 in the UHV chamber. Spectra were collected using 7 mW of $\lambda_{ex} = 514.5$ nm collected for 30 s.

measured is approximately 0.44 and may be considered "clean" (i.e., surface carbon concentration is less than 1%).

In the UHV−SERS experiments described above for pyridine and benzene, the maximum surface temperature was typically 350 K. In the case of pyridine, a small SERS peak at 998 cm^{-1} persisted even after desorption at 350 K (Figure 8A), and its intensity remained constant over many adsorption−desorption cycles. A high temperature molecular desorption peak for pyridine was also detected by TPD at 450 K, and a likely postulate is that its desorption can be attributed to an α-pyridyl radical species formed upon dissociative chemisorption[49] (Figure 8B). Although sample to sample SERS intensity variations were observed, the majority of AgFON surfaces did not lose their enhancement even after heating to surface temperatures of ∼500 K in an attempt to desorb the hypothesized α-pyridyl radical species.

The thermal desorption of C_{60} from the AgFON surface is explored in Figure 9. The SERR spectrum of 0.1 ML of C_{60} adsorbed on a fresh surface (Figure 9A) (same sample as that shown in Figure 6B) is compared with that of residual C_{60} after desorption at 573 K (Figure 9B). These experiments demonstrate the thermal stability of the AgFON surface and indicate that SERS can be used in vibrational studies at higher temperatures than previously thought feasible.

In Figure 10, the AFM image and reflectance mode UV−vis extinction spectra of a newly prepared AgFON surface at 300, 350, 473, and 548 K are shown. The AFM images clearly show an increased areal density of smaller scale nanostructures after annealing to 350 K. A subsequent reduction in the areal density of these smaller nanostructures is seen upon annealing to 473 and 548 K. The intensity of the UV−vis extinction peak increases after annealing to 350 K and approximately tracks that areal density of the small nanostructures. As the smaller

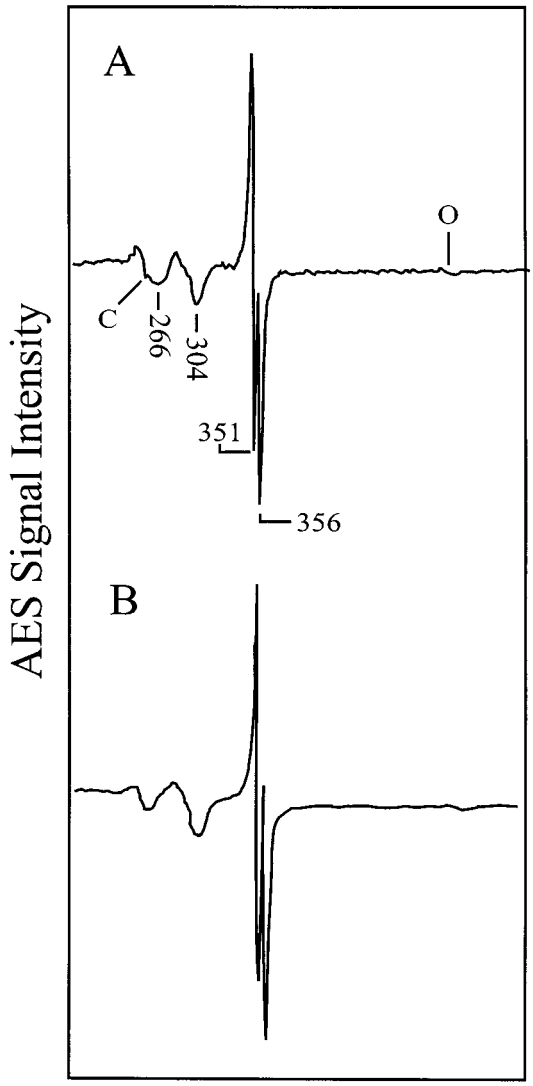

Figure 7. AES of the AgFON surface in the 200−600 eV region. (A) Before any adsorbate was deposited and (B) after many adsorption−desorption cycles of benzene and pyridine.

nanostructures coalesce, the intensity of the UV−vis extinction signal is concomitantly reduced.

Regeneration of AgFON Surfaces. An experiment designed to regenerate the SERS activity of a "used" AgFON surface by sputter cleaning and annealing is shown in Figure 11. The SER spectrum of pyridine on a new AgFON surface (Figure 11A) is compared to the SER spectrum of freshly dosed pyridine on a regenerated AgFON surface (Figure 11B). (The small peak at ∼960 cm^{-1} in Figure 11B, indicated by the asterisk, is due to benzene-d_6 inadvertently coadsorbed with pyridine). Although the SER intensity on the regenerated surface is a factor of 2 less than that on the freshly deposited surface, it is clear that sufficient signal is available following regeneration to permit useful UHV−SERS experiments.

Conclusions

Silver film over silica nanospheres, AgFON, surfaces are effective SERS-active substrates for use in ultrahigh vacuum (UHV). Three different adsorbates (viz. benzene, pyridine, and C_{60}) were used to probe the characteristics of the AgFON surface. Benzene was found to adsorb parallel to the silver surface as is commonly observed, but the SER spectra also demonstrate the coexistence of a perpendicular adsorption

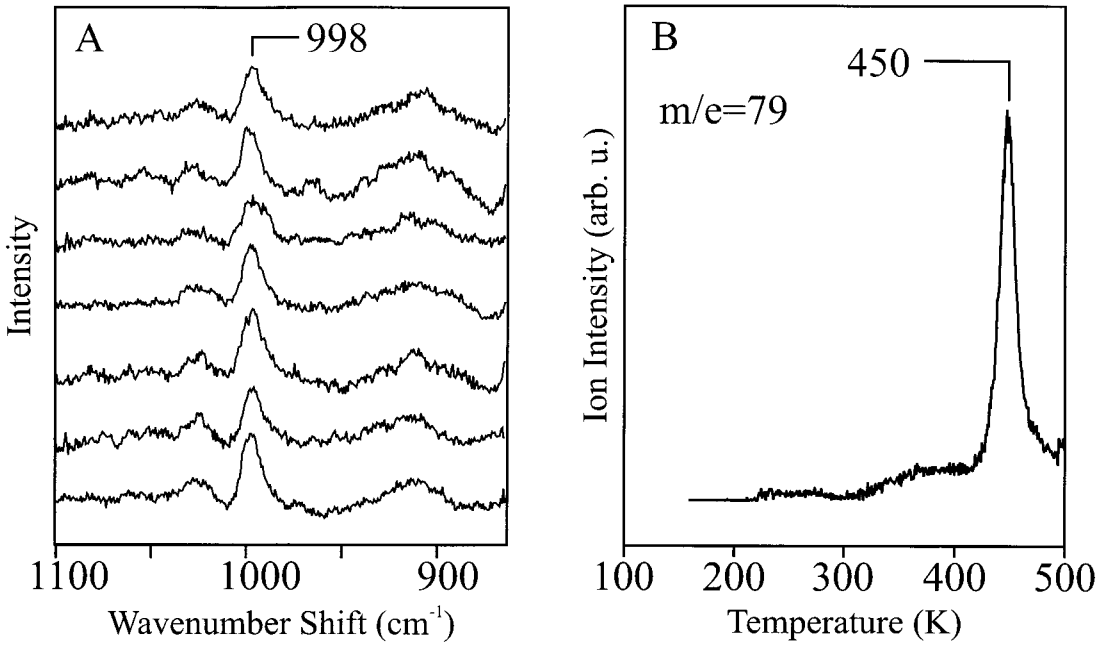

Figure 8. SER and TPD spectra of chemisorbed pyridine. (A) SER spectra of residual pyridine on a AgFON surface after each adsorption−desorption cycle. Spectra were taken with 8 mW of $\lambda_{ex} = 632.8$ nm for 60 s. (B) TPD spectrum of the residual pyridine collected with $\beta = 4$ Ks^{-1}.

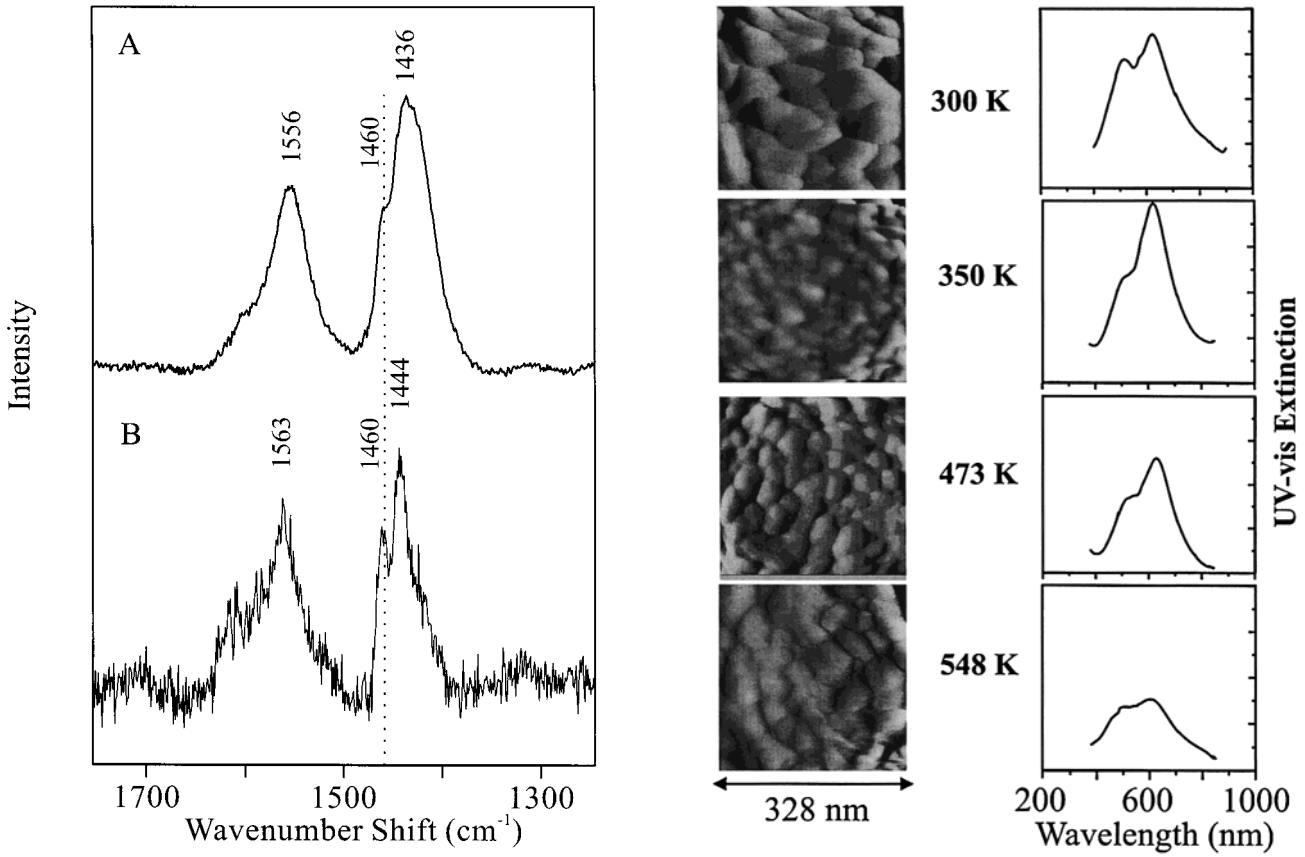

Figure 9. SERR spectra of C_{60}. (A) SERR spectrum of 0.1 ML of C_{60} freshly deposited on a AgFON surface. (B) SERR spectrum of the AgFON surface after 1.0 ML of C_{60} was thermally desorbed to 573 K. The spectra were taken with 7 mW of $\lambda_{ex} = 514.5$ nm for 30 s.

Figure 10. AFM image and UV−vis extinction spectra of a stepwise annealing process of the AgFON surface. Images were captured after annealing the sample for 30 min at 300, 350, 473, and 548 K.

geometry, thought to occur at step edges and defect sites. The combined SERS and TPD data demonstrate that physisorbed and chemisorbed pyridine coexist on the AgFON substrate. High-temperature SERS/TPD studies were performed using C_{60} adsorption. The measured SER spectra mimic results previously thought to be anomalous and suggest that previously published C_{60} SER spectra are actually C_{60}^- SER spectra. All three adsorbate studies give evidence that the AgFON surface is an effective SERS-active, UHV compatible substrate with the following desirable properties: (1) the film over nanospheres substrate is a materials general, reproducible, and cost-effective SERS-active substrate; (2) the surface is temporally stable; and (3) surface regeneration is easily achieved on this SERS-active

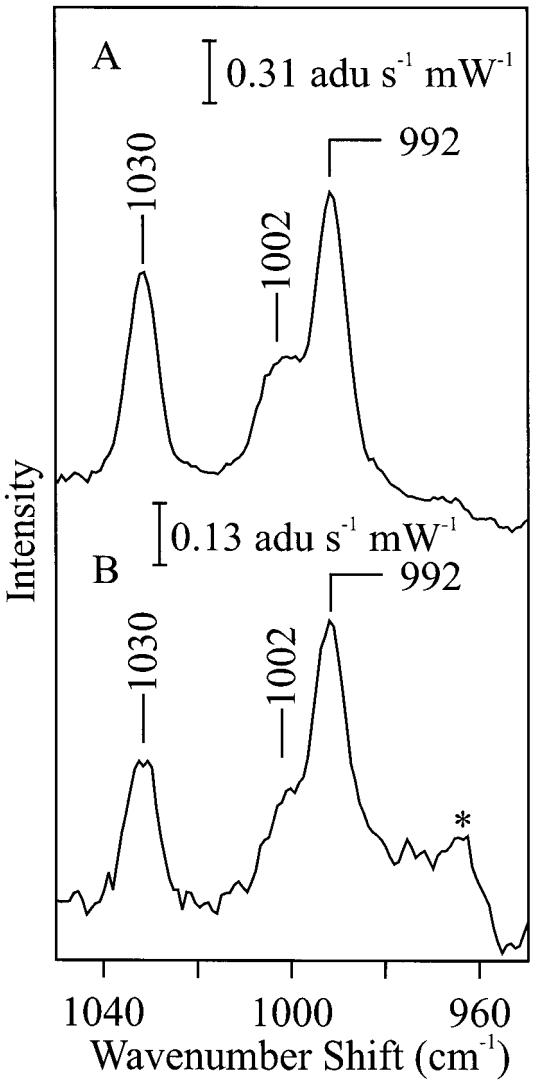

Figure 11. Regeneration of the AgFON surface. (A) SER spectra of 5 L of pyridine on a new AgFON surface. (B) AgFON surface which has been Ar-ion sputtered for 3 h at 1 kV, annealed to 573 K for 2 h, and then redeposited with 120 nm of silver. Spectra were taken with 18 mW of $\lambda_{ex} = 514.5$ nm for 200 s.

surface that does not show irreversible loss. The thermal stability of the AgFON surface argues against an adatom interpretation of the SERS chemical enhancement mechanism of the AgFON substrate. Measured UV−vis extinction spectra show that structural changes occurring as a result of increasing surface temperature diminish the intensity of the localized surface plasmon resonance (LSPR). The coincident decrease of SERS activity with the decreasing LSPR intensity supports the dominant role of the electromagnetic enhancement mechanism in explaining SERS.

Acknowledgment. We gratefully acknowledge NSF (Grant No. CHE-940078) for financial support. We thank Professor Peter Stair and his group for help in implementing TPD.

References and Notes

(1) Weaver, M. J.; Zou, S. Vibrational Spectroscopy of Electrochemical Interfaces: Some Walls and Bridges to Surface Science Understanding. In *Spectroscopy for Surface Science*; Clark, R. J. H., FRS, Hester, R. E., Eds.; John Wiley & Sons: New York, 1998; Vol. 26; pp 219−272.

(2) Campion, A.; Kambhampati, P. *Chem. Soc. Rev.* **1998**, *27*, 241−250.

(3) Otto, A.; Mrozek, I.; Grabhorn, H.; Akemann, W. *J. Phys. Condens. Matter* **1992**, *4*, 1143−1212.

(4) Cotton, T. M.; Brandt, E. S. Surface-Enhanced Raman Scattering. In *Physical Methods of Chemistry Series: Investigations of Surfaces and Interfaces−Part B*, 2nd ed.; Rossiter, B. W., Baetzold, R. C., Eds.; John Wiley & Sons: New York, 1993; Vol. IXB.; pp 633−718.

(5) Moskovits, M. *Rev. Mod. Phys.* **1985**, *57*, 783−826.

(6) Weaver, M. J. *J. Phys. Chem.* **1996**, *100*, 13 079−13 089.

(7) Nabiev, I.; Chourpa, I.; Manfait, M. *J. Raman Spectrosc.* **1994**, *25*, 13−23.

(8) Fabian, H.; Anzenbacher, P. *Vib. Spectrosc.* **1993**, *4*, 125−148.

(9) Douketis, C.; Haslett, T. L.; Wang, Z.; Moskovits, M.; Iannotta, S. *Prog. Surf. Sci.* **1995**, *50*, 187−195.

(10) Van Duyne, R. P.; Haller, K. L.; Altkorn, R. I. *Chem. Phys. Lett.* **1986**, *126*, 190−196.

(11) Kneipp, K.; Kneipp, H.; Itzkan, I.; Dasari, R. R.; Feld, M. S. *Chem. Rev.* **1999**, *99*, 2957−2975.

(12) Hildebrandt, P.; Stockburger, M. *J. Phys. Chem.* **1984**, *88*, 5935−5944.

(13) Schatz, G. C. Electromagnetic Mechanism of Surface Enhanced Spectroscopy. In *Fundamentals and Applications of Surface Raman Spectroscopy*; Garrell, R. L., Pemberton, J. E., Cotton, T. M., Eds.; VCH Publishers: Deerfield Beach, Florida, 1997.

(14) Kambhampati, P.; Child, C. M.; Foster, M. C.; Campion, A. *J. Chem. Phys.* **1998**, *108*, 5013−5026.

(15) Michaels, A. M.; Nirmal, M.; Brus, L. E. *J. Am. Chem. Soc.* **1999**, *121*, 9932−9939.

(16) Emory, S. R.; Haskins, W. E.; Nie, S. *J. Am. Chem. Soc.* **1998**, *120*, 8009−8010.

(17) Michaels, A. M.; Jiang, J.; Brus, L. *J. Phys. Chem. B* **2000**, *104* (*50*), 11965−11971.

(18) Smardzewski, R. R.; Colton, R. J.; Murday, J. S. *Chem. Phys. Lett.* **1979**, *68*, 53−57.

(19) Eesley, G. L.; Smith, J. R. *Solid State Commun.* **1979**, *31*, 815−819.

(20) Rowe, J. E.; Shank, C. V.; Zwemer, D. A.; Murray, C. A. *Phys. Rev. Lett.* **1980**, *44*, 1770−1773.

(21) Wood, T. H.; Zwemer, D. A.; Shank, C. V.; Rowe, J. E. *Chem. Phys. Lett.* **1981**, *82*, 5−8.

(22) Sanda, P. N.; Demuth, J. E.; Tsang, J. C.; Warlaumont, J. M. Coverage Dependence. In *Surface Enhanced Raman Scattering*; Chang, R. K., Furtak, T. E., Eds.; Plenum Press: New York, 1982; pp 189−202.

(23) Tsang, J. C.; Kirtley, J. R.; Theis, T. N. *J. Chem. Phys.* **1982**, *77*, 641−645.

(24) Seki, H. *J. Vac. Sci. Technol.* **1981**, *18*, 633−637.

(25) Seki, H. *J. Chem. Phys.* **1982**, *76*, 4412−4418.

(26) Seki, H.; Philpott, M. R. *J. Chem. Phys.* **1980**, *73*, 5376−5379.

(27) Mrozek, I.; Pettenkofer, C.; Otto, A. *Surf. Sci.* **1990**, *238*, 192−198.

(28) Royer, P.; Goudonnet, J. P.; Warmack, R. J.; Ferrell, T. L. *Phys. Rev. B* **1987**, *35*, 3753−3759.

(29) Roark, S. E.; Rowlen, K. L. *Chem. Phys. Lett.* **1993**, *212*, 50−56.

(30) Van Duyne, R. P.; Hulteen, J. C.; Treichel, D. A. *J. Chem. Phys.* **1993**, *99*, 2101−2115.

(31) Norrod, K. L.; Rowlen, K. L. *Anal. Chem.* **1998**, *70*, 4218−4221.

(32) Seki, H.; Chuang, T. J. *Solid State Commun.* **1982**, *44*, 473−475.

(33) Pockrand, I.; Otto, A. *Solid State Commun.* **1981**, *38*, 1159−1163.

(34) Wood, T. H.; Klein, M. V.; Zwemer, D. A. *Surf. Sci.* **1981**, *107*, 625−635.

(35) Pockrand, I.; Otto, A. *Solid State Commun.***1980**, *35*, 861−865.

(36) Wood, T. H.; Klein, M. V. *Solid State Commun.* **1980**, *35*, 263−265.

(37) Douketis, C.; Wang, Z.; Haslett, T. L.; Moskovits, M. *Phys. Rev. B* **1995**, *51*, 11022−11031.

(38) Reed, C. E.; Giergiel, J.; Ushioda, S.; Hemminger, J. C. *Phys. Rev. B* **1985**, *31*, 1873−1880.

(39) Zou, S.; Weaver, M. J.; Li, X. Q.; Ren, B.; Tian, Z. Q. *J. Phys. Chem. B* **1999**, *103*, 4218−4222.

(40) Luo, H.; Weaver, M. J. *Langmuir* **1999**, *15*, 8743−8749.

(41) Zou, S.; Williams, C. T.; Chen, E. K.-Y.; Weaver, M. J. *J. Am. Chem. Soc.* **1998**, *120*, 3811−3812.

(42) Zou, S.; Weaver, M. J. *Anal. Chem.* **1998**, *70*, 2387−2395.

(43) Williams, C. T.; Takoudis, C. G.; Weaver, M. J. *J. Phys. Chem. B* **1998**, *102*, 406−416.

(44) Zou, S.; Gomez, R.; Weaver, M. J. *Langmuir* **1997**, *13*, 6713−6721.

(45) Liao, P. F.; Bergman, J. G.; Chemla, D. S.; Wokaun, A.; Melngailis, J.; Hawryluk, A. M.; Economou, N. P. *Chem. Phys. Lett.* **1981**, *81*, 355−359.

(46) Hulteen, J. C.; Van Duyne, R. P. *J. Vac. Sci. Tech. A* **1995**, *13*, 1553−1558.

(47) Hallmark, V. M.; Campion, A. *Chem. Phys. Lett.* **1984**, *110*, 561−564.

(48) Wolkow, R. A.; Moskovits, M. *J. Chem. Phys.* **1986**, *84*, 5196−5199.
(49) Haq, S.; King, D. A. *J. Phys. Chem.* **1996**, *100*, 16 957−16 965.
(50) Litorja, M. *Surface-Enhanced Raman Spectroscopy and Temperature Programmed Desorption of Benzene, Pyridine, and C_{60}*. Ph.D. Thesis, Northwestern University, 1996.
(51) Litorja, M.; Van Duyne, R. P. *J. Phys. Chem. B*, in preparation.
(52) Mullins, D. R.; Campion, A. *Chem. Phys. Lett.* **1984**, *110*, 565−570.
(53) Pockrand, I. *Chem. Phys. Lett.* **1982**, *92*, 514−518.
(54) Akers, K. I.; Cousins, L. M.; Moskovits, M. *Chem. Phys. Lett.* **1992**, *190*, 614−620.
(55) Zhang, Y.; Edens, G.; Weaver, M. J. *J. Am. Chem. Soc.* **1991**, *113*, 9395−9397.
(56) Caldwell, W. B.; Chen, K.; Herr, B. R.; Mirkin, C. A.; Hulteen, J. C.; Van Duyne, R. P. *Langmuir* **1994**, *10*, 4109−4115.
(57) Kelemen, S. R.; Wachs, I. E. *Surf. Sci.* **1980**, *97*, L370−L374.